

Carbon dioxide precedes temperature change during short-term pauses in multi-millennial palaeoclimate records



Knut L. Seip^{a,*}, Øyvind Grøn^a, Hui Wang^b

^aOsloMet - Oslo Metropolitan University, Pilestredet 35, N-0130 Oslo, Norway

^bNOAA/NWS/NCEP/Climate Prediction Center, 5830 University Research Court, NCWCP, College Park, MD 20740, USA

ABSTRACT

In Antarctica, ice-core temperature has traditionally been regarded as a leading variable to carbon dioxide, CO₂ during the last 400,000 years before present (B.P.). This finding is in contrast to most reports on global mean surface temperature and atmospheric CO₂ for the last 150 years. However, previous techniques for establishing leading or lagging (LL) relations between paired global warming variables have required that the time series show constant frequency (stationarity). Herein, we show that on orbital and multi-millennial time scales, the Vostok Antarctic ice core displays 9 periods of 8.7 kyr ± 5 kyr during which CO₂ becomes a leading variable to temperature. Six of the 9 periods were associated with short-term pauses occurring during 4 major glaciation-deglaciation periods. We find that CO₂ also leads temperature during short pauses in the major cyclic pattern of the Greenland time series. In the latter series, there are also two contrasting cycle developments. In the first contrasting cycle developments, lasting from 103.5 to 79 ka, there is an in-phase relation between CO₂ and temperature, with a slope of 0.75. In the second contrasting cycle developments, lasting from 61.5 to 43.5 ka, there is an out-of-phase relation with a slope of -0.67. In addition, the latter shows a see-saw pattern between Arctic and Antarctic temperatures.

1. Introduction

The question of whether increasing CO₂ will lead or lag global warming is relevant for the interpretation of candidate factors that cause changes in the global mean temperature. It is relevant on the palaeontological 100,000 year scale, the millennial scale, and the present 100-year time scale (Cuffey and Vimeux, 2001; Barker et al., 2011; Seip and Grøn, 2017a, 2017b). Here, we examine leading and lagging (LL) relations on the orbital and multi-millennial time scales.

Antarctic temperature appears to have been a leading or synchronous variable to CO₂ during the last 800 kyr (Cuffey and Vimeux, 2001; Monnin et al., 2001; Stips et al., 2016). On a millennial, global scale, CO₂ appears to be a leading variable to temperature on average during the last deglaciation period but not at its onset (Shakun et al., 2012).

An important issue is whether it is possible to find the mechanisms that trigger deglacial warming (Imbrie et al., 1993; Shakun et al., 2012; He et al., 2013). These studies suggest that Milankovitch cycles may induce global warming (≈ 3 °C), which initiates ice melting and subsequent increases in CO₂ concentrations that further provide means for global deglaciation. The present study gives a more detailed picture of LL relations between temperatures, CO₂, and CH₄ during the four recent

glaciation-deglaciation cycles.

We apply a local method for identifying LL relations. The method distinguishes itself from alternative methods in that it can be used to calculate LL relations for three consecutive observations in paired time series and makes it possible to find significant LL relations at the 95% level for 9 consecutive observations. The method does not require observations to be equally spaced or that the series show constant frequency (showing stationarity), but the observations in the paired series have to be sampled at the same time steps (being synoptic).

Since both CO₂ and global mean temperature time series appear to result from several cyclic phenomena, it may be that there are cycles that result from interactions between global surface temperature (GST) and a series of dynamical systems: i) the Solar system (He et al., 2013; Ma et al., 2017), ii) the atmosphere (Knutson et al., 2015), iii) the oceans, including ice-sheets (Barker et al., 2011; He et al., 2013; DeVries et al., 2017) and biogenic carbonate and ocean fertilization (Tang et al., 2016), iv) the Earth's core, e.g., directly through magma migration (Stevens et al., 2016) or through volcanic activities (Huybers and Langmuir, 2009; Huybers and Langmuir, 2017) that affect the CO₂ emissions, and v) anthropogenic substances that are brought into the atmosphere. Since CO₂ and temperature are either synchronous or show

* Corresponding author.

E-mail addresses: knut.lehre.seip@OsloMet.no (K.L. Seip), oyvind.gron@OsloMet.no (Ø. Grøn), hui.wang@noaa.gov (H. Wang).

LL relations between them, identifying common patterns may also help in identifying common governing mechanisms.

In the present study, we examine and compare LL relations between CO₂ and global temperature anomalies (TEMP) for three datasets: i) a 400 kyr dataset from the Vostok ice core in Antarctica, ii) a 120 kyr dataset from the NGRIP ice core in Greenland, and iii) a composite 20-kyr dataset, which represents a global mean for the last deglaciation period constructed by Shakun et al. (2012). There are several recent potential improvements to the records, e.g., those reported by Buizert et al. (2015) and Parrenin et al. (2013). To test the robustness of our results, we repeat selected calculations with the dataset of Parrenin.

Our first hypothesis to be tested is that CO₂ changes may sometimes lead and at other times lag temperature changes in the time series. The rationale is that we believe cycles in the series are caused by interactions within the oceans or between the oceans and the atmosphere so that there will be net sequestering of CO₂ during some periods and net emissions of CO₂ during other periods, e.g., “Tang et al. (2016)”. Sequestering and emissions of CO₂ may not be a direct function of ocean temperature but may be indirect effects of winds set up by regional temperature differences. Other mechanisms may also be important, e.g., those discussed in Patra et al. (2005) and Johnston and Alley (2006). Furthermore, we hypothesize that the time windows when CO₂ leads temperature can be associated with characteristic events in the temperature series.

Our second hypothesis to be investigated is that the relation between the LL patterns that we find for the four-glaciation periods in Antarctica will also be found for the glaciation-deglaciation period in the Arctic and in the global deglaciation pattern identified by Shakun et al. (2012).

Third, we examine if there are anti-phase or see-saw patterns on the multi-millennial scales. The rationale is that such patterns have been found on millennial (Stocker, 1998) and decadal (Chylek et al., 2010) scales.

The rest of the paper is organized as follows. In Section 2 we present the material, and in Section 3 we provide an outline of the method used to identify leading, lagging and synchronous relations between paired cyclic time series. In Section 4 we show results for the sets of time series for Antarctica, the Arctic, and the globe. In Section 5 we discuss the results, and our results are summarized in Section 6.

2. Materials

Herein, we examine time series for Antarctica, the Arctic represented by Greenland and a synthetic series set for the globe. The first series describes four glaciation periods in Antarctica. The data were retrieved from “<https://www.ncdc.noaa.gov/paleo-search/study/15076>”, and we used the “<http://www1.ncdc.noaa.gov/pub/data/paleo/icecore/antarctica/aicc2012icecore-data.xls>” data file with δD (‰) based on Petit et al. (1999). The temperature data span the period 400 ka–3 ka and were based on analyses of the Vostok ice core. The median value for the time steps was 85 years. The CO₂ data were retrieved from <https://www.ncdc.noaa.gov/paleo-search/study/15076> as well and are due to Luthi et al. (2008), transferred on AICC2012. The period for the CO₂ values was from 350 years (B.P. 1950) to 798.6 ka. The data were unequally spaced, with time steps ranging from 0 to 6.01 kyr and median value of 590 years. The time intervals are shown as histograms in Supplementary material 1. The data were linearly interpolated to a 500-yr resolution. Carbon dioxide and temperature data for Antarctica from Parrenin et al. (2013) were retrieved from the article's Supplementary material. We did not use the time series from 800 ka to 400 ka because the time resolution is much coarser for those data. The methane data were retrieved from “Petit et al. (1999)”. These data correspond well with data retrieved from the EDC record for the last 420 kyr (Loulergue et al., 2008). The period for the CH₄ values was from 6.6 ka to 403.7 ka. The data for CH₄ were also unequally spaced, with a median time step of 404 yrs. The data were

linearly interpolated to the 500-yr resolution.

The second series describes a glaciation-deglaciation period in Greenland. The data were retrieved from <https://www.ncdc.noaa.gov/paleo-search/study/15076>. The temperature data span the period 120 ka to –30 yr (B.P.). The time steps were unequally spaced, with time steps ranging from 14 to 25 years and median time step of 20 years. The $\delta^{18}O$ ice (‰) values ranged from 46.5 yr to 32.1 yr, with a median value of 40 yr. There are no CO₂ records for Greenland because CO₂ cannot be measured with accuracy in ice-cores from Greenland (Barnola et al., 1995). In addition to the temperature records, there is also a record for methane from Petit et al. (1999) that starts at 119.673 years (B.P.) and ends at 89.453 years (B.P.). However, there is a vacancy in the series from 100.201 years (B.P.) to 62.960 years (B.P.). The data were transformed to synoptic series using linear interpolation with a 500-yr resolution.

The third series describes the last global deglaciation period. The data were supplied by Shakun (personal communication) but can be found in <http://www.nature.com/nature/journal/v484/n7392/full/nature10915.html>. The data span the period 22 ka–6.5 ka and were calculated as the area-weighted mean of 80 globally distributed temperature records with median resolution of 200 yr. The resulting series was linearly interpolated to a 100-yr resolution to agree with Shakun et al. (2012) and to the 500-yr resolution to be consistent with the other series. The sets we used for Antarctica and the Arctic are shown as raw series in Fig. 1A and as smoothed series in Fig. 1B. Fig. 1C and D will be discussed later.

The temperature data were obtained from the stable isotope compositions of water in the ice cores (δD or $\delta^{18}O$) used as a proxy. Because we only examined LL relations between the temperature, CO₂ and CH₄, we normalized all the time series to unit standard deviation and thus did not convert the proxies to temperatures. However, we use the terms temperature, or TEMP, CO₂ and CH₄ to ease reading. We adopt the term “short-term pauses” when the time series on orbital or multi-millennial scale appear to show a pause, although there may still be small amplitude oscillations. We use the Greek letter β for the slopes between x- and y-variables.

3. Methods

Several methods are available to establish cause and effect relations (Granger, 1969; Sugihara et al., 2012; Stips et al., 2016). However, causality requires that the cause comes before the effect, and several studies restrict the topic to potential causality and require physical, chemical and biological plausibility for support. Kestin et al. (1998) provide an overview of methods, and Huang et al. (1998) describe the identification of moving frequencies. Alley et al. (2002) discuss advantages of identifying maxima or minima in contrast to midpoints in global warming time series. We adopt a method developed by Seip and Grøn (2017a, 2017b), which determines LL relations for paired synoptic series of three consecutive observations.

3.1. The leading-lagging (LL) method

The method consists of 5 steps that are explained below with reference to Fig. 2. This explanation follows closely the description given in Seip and Grøn (2016). The first part of the method, step 2 below, has a counterpart in electrical engineering in Lissajous curves, see, e.g., https://en.wikipedia.org/wiki/Lissajous_curve. The second part, step 3 and Eq. (1), has a counterpart in the calculation of magnetic fields around a wire, e.g., <https://en.wikipedia.org/wiki/Biot%20and%20Savart%20law>.

In step 1, we centralize and then normalize the data to unit standard deviation. In this step, we also smooth the series to avoid singularities in the subsequent calculations. With smoothing, we also see trends in the data more clearly (see the Detrending and smoothing section below).

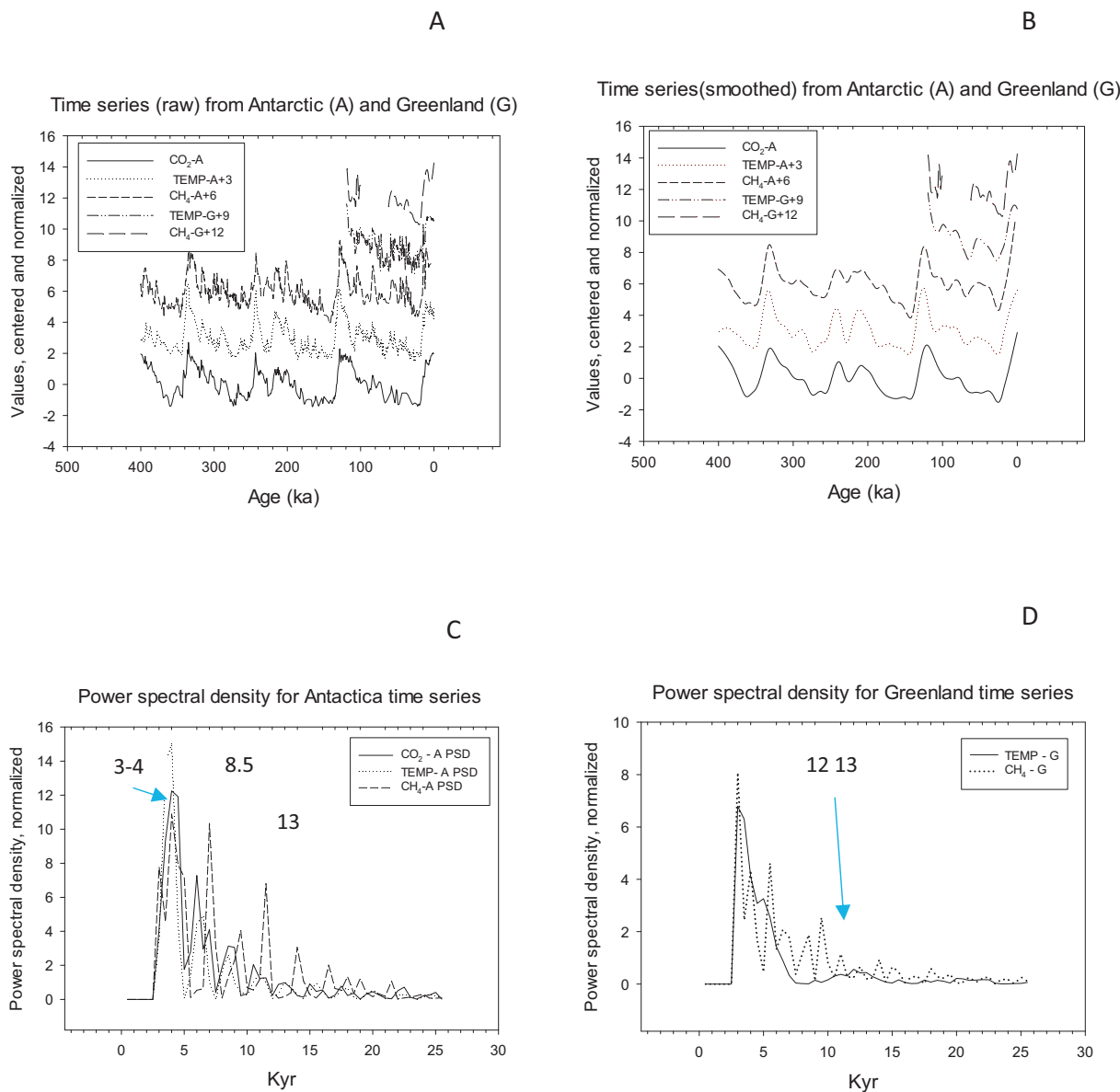


Fig. 1. Time series characteristics. A. Time series from the Antarctic and Greenland normalized to unit standard deviation. B. Time series for Greenland and the Antarctic smoothed. C. Power spectral density for Antarctica time series. For the Antarctic, CO₂ has peaks at 3–4 kyr, 8.5 kyr, and 11.5 kyr, TEMP has peaks at 4 kyr, 8.5 kyr and 13 kyr, and CH₄ has peaks at 4 kyr, 7 kyr and 11.5 kyr. D. For Greenland, TEMP has peaks at 3 kyr, 5 kyr, and 12–13 kyr, and CH₄ has peaks at 3 kyr, 5.5 kyr, 6.5 kyr, 8.5 kyr and 11 kyr.

In step 2, we illustrate the method with sampled sine functions, $x = \sin(0.5t)$, leading the candidate target sine function, $y = \sin(0.5t - \varphi \text{ RAND}())$, where $\varphi = \pi/4$, and $\text{RAND}()$ is a random component. The random component makes the example slightly more realistic (Fig. 2A). With the candidate leading sine function, $x = \sin(0.5t)$, on the x-axis, and the candidate target sine function, $y = \sin(0.5t - \varphi \text{ RAND}())$, where $\varphi = \pi/4$, on the y-axis, the rotation in a phase plot will largely be counterclockwise, as shown in Fig. 2B. The angles θ between two successive trajectories are shown as black bars in Fig. 2C. In the example, the candidate leading series on the x-axis is almost consistently leading the target series on the y-axis with a phase shift of $\pi/4$. The light gray bars denote LL strength averaged over $n = 5$ observations (because the sample is short), and the dashed lines suggest confidence limits for $n = 9$.

In step 3, we calculate LL relations. We give the LL relationship a numerical representation. To see which variable peaks first, we quantify rotational directions, θ , with the formula (c.f., Supplementary material 2)

$$\theta = \text{sign}(\mathbf{v}_1 \times \mathbf{v}_2) \text{Arccos} \left(\frac{\mathbf{v}_1 \cdot \mathbf{v}_2}{|\mathbf{v}_1| |\mathbf{v}_2|} \right). \quad (1)$$

Here, \mathbf{v}_1 and \mathbf{v}_2 are two consecutive trajectory vectors in the phase diagram, and \times denotes the vector product. In step 4, we calculate the LL strength of the mechanisms that cause two variables to rotate either clockwise or counterclockwise in a phase portrait. It is measured by the number of positive rotations (counterclockwise rotations by convention) minus the number of negative rotations, relative to the total number of rotations over a certain period, 9 time steps in this study:

$$\text{LL} = (N_{\text{pos}} - N_{\text{neg}}) / (N_{\text{pos}} + N_{\text{neg}}). \quad (2)$$

We use the nomenclature $\text{LL}(x, y) = [-1, 1]$ for LL strength; $\text{LL}(x, y) < 0$ implies that y leads x , $y \rightarrow x$, and $\text{LL}(x, y) > 0$ implies that x leads y , $x \rightarrow y$. The LL strength for the series in Fig. 2A is equal to 0.49 on a scale from -1 to $+1$. Thus, we can use the rotational directions in phase plots for two cyclic series to infer which series precedes the other in the sense that its peak (trough) is less than $1/2$ of a cycle length before

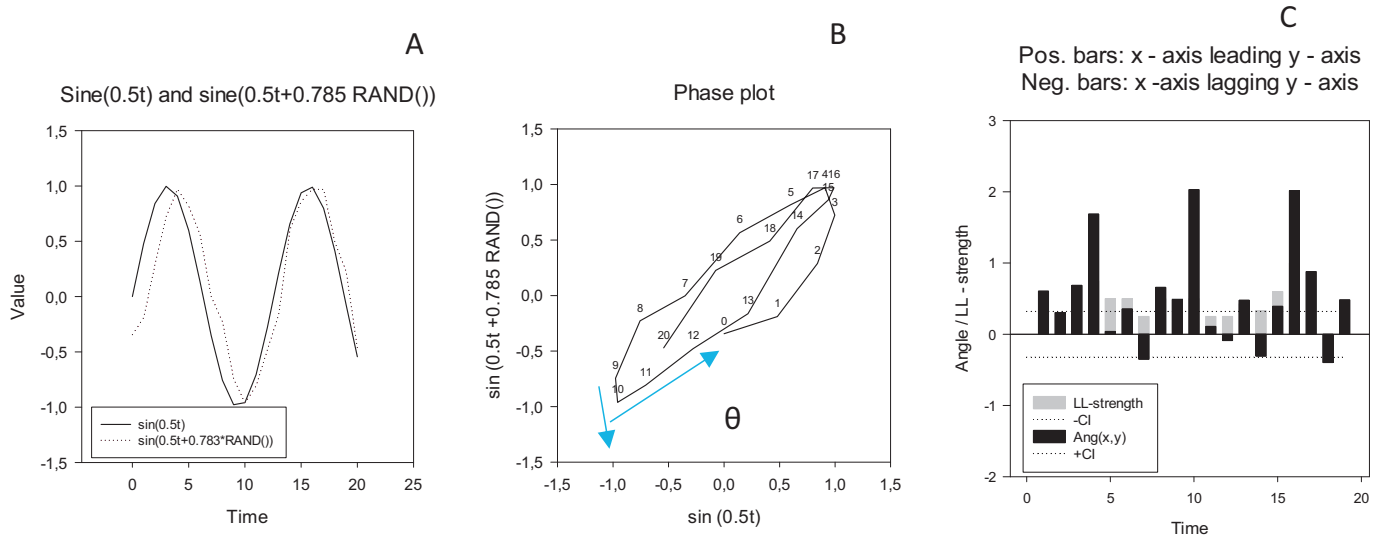


Fig. 2. Example. Calculating leading-lagging (LL) relations and LL strength A. Two sine functions; the full line function is a candidate cause, and the dashed line function is the target. The candidate cause generally peaks before the target. B. In a phase plot with the candidate cause on the x-axis and candidate target on the y-axis, the time series rotates counterclockwise (negative by definition), and θ is the angle between two consecutive trajectories. Note that for paired perfect sine functions, the phase plot will be elliptical with a center in the origin and the long axis with the direction 1:1 or 1: -1. See the text for details. C. Angles between successive trajectories (black bars) and LL strength (gray bars). The dashed lines suggest confidence limits for persistent rotation in the phase plot and persistent leading or lagging relations in the time series plot.

the peak (trough) of the other. However, the LL relations apply to all sections of the time series of 3 consecutive steps or longer. In the calculations, we measure time before present (B.P., 1950) as negative. The rule will therefore be that the x-axis variable leads the y-axis variable when there is a clockwise rotation. The LL strength passes through non-significant LL portions of the time series when LL relations change sign. Since the palaeoclimate see-saw relation between the Northern and Southern Hemisphere temperature series focuses on phase relationships or phase shifts (PS; e.g., Stocker and Johnsen (2003)), we here apply the nomenclature that paired series are in antiphase, or counter cyclic, if $\frac{1}{4} \lambda < PS < \frac{3}{4} \lambda$, that is, the slope is negative when the two series are plotted in a phase plot.

The measured LL strength captures two aspects of the LL relationship between paired variables. It obtains a high/low value when one series is consistently leading or lagging the other. However, to obtain a high/low value, the two series have to change cycle lengths in concert.

The cycle length (CL) of two paired series can be approximated with two methods. With the *partial ellipse* method, CL can be approximated as (Seip and McNown, 2007)

$$CL = n \times 2\pi / \left(\sum_2^{n-1} \theta_{i-1,i,i+1} \right). \quad (3)$$

Here, $\theta_{i-1,i,i+1}$ are angles between successive trajectories, and n is the number of points sampled. The cycle lengths should ideally be based on full rotations in the phase plots for the paired time series, but noise or other superimposed signals may not allow full rotations to be completed as a significant series. With two perfect sines (no random component added in Fig. 2), $CL = \lambda = 6.30$, which is close to the design cycle length of $\lambda = 2\pi \approx 6.28$. The angles with a phase shift of $\lambda/2$ give an average angle of -1.00 ± 0.00 rad. With a phase shift of $\lambda/4$, the average angle is -1.07 ± 0.48 ; that is, the rotational pattern is an ellipse. We then get the same average angle, but with greater standard deviation.

The *cumulative angle* method provides estimates of cycle lengths by a calculation of the cumulative angles in phase space and then terminates the calculations when the sum reaches 2π . The cycle length is equal to the number of angles and time steps at this cut off value. For time series where one series is a superposition of two sine functions with different cycle lengths and the other series represents one of the sine functions in

the superposition, the method extracts the common cycles for the two series.

For cyclic series, the regression slopes, s , or the β -coefficients provide information on the shift or time lag between the series. For a linear regression applied to paired time series that are normalized to unit standard deviation, the regression coefficient, r , and the β -coefficient will be identical. If the two series co-vary exactly, their regression coefficient will be 1, and the time lag zero. If they are displaced half a cycle length, $\lambda/2$, the series are counter-cyclic, and the regression coefficient is $r = -1$. Lead or lag times, or phase shift (PS), are estimated from the regression coefficient, r , for sequences of 5 observations, PS (5). With λ as cycle length, the phase shift between two cyclic series can be approximated by the expression

$$PS \approx \lambda/2\pi \times (\pi/2 - \text{Arcsine}(r)). \quad (4)$$

For $r = 1$, $\text{Arcsine}(r) = \pi/2$, the right hand parenthesis is zero, giving $PS = 0$. For $r = -1$, $\text{arcsine}(r) = -\pi/2$, the right hand parenthesis is $2 \times \pi/2 = \pi$, and $PS = \lambda/2$.

In step 5, we design a graphical presentation of the results in terms of rotational angles between trajectories in the phase plot.

3.2. Significance

The number of angles that has to rotate in the same direction for the LL relation to be significant was found by applying Eq. (3) to two series of 9 observations generated by Monte Carlo simulations. The number 9 is a tradeoff between the possibility of finding local LL relations and determining confidence levels. The LL strength of a time series is significant at the 95% level if the LL strength < -0.32 or the LL strength $> +0.32$.

3.3. Detrending and smoothing

When detrending a time series, it is usual to apply linear detrending to minimize shifting the series along the time-axis. However, a second order polynomial detrending may show satisfactory results for series with progressively increasing trends. There is no canonical way to smooth data to identify with certainty movements that are the result of a given cause and its effect. In particular, if the series contains dynamic

chaos, identifying component series that represent causes and effects may be difficult (Ellner and Turchin, 2005). However, several methods have been used to identify embedded series that correspond to real processes (Huang et al., 1998; Alley et al., 2002; Wu et al., 2011; Kawamura et al., 2017). Here, we apply the LL method to the smoothed data. The smoothed sets represent movements that to our best knowledge minimize noise. Additionally, we examined if the smoothed series exhibited patterns that are reported for the series elsewhere in the literature (e.g., Barker et al. (2011); Alley et al. (2002)). Lastly, the LL method identifies common cycles between paired series, and when those cycles are longer than 7 time steps, the probability that they occur by chance is less than $p = 0.05$ (Seip and Grøn (2016)), supporting the hypothesis that the smoothed series represent real processes. We smoothed the series with the LOESS algorithm in SigmaPlot®, using fractions $f = 0.07$ to 0.2 of the series and a 2nd order polynomial function for interpolation.

3.4. Power spectral density (PSD)

PSD methods will show cycle lengths for single series, and those cycles can be compared to the cycles obtained with the LL method. Power spectral analysis is undertaken using the standard method found in SigmaPlot®. We stack PSD curves from several series and use the peaks found in the stacks for comparison with cycle lengths found with the LL method. We do not perform a formal uncertainty analysis, but the peaks found in the stacked PSD are higher than peaks that would result from PSD analysis of a comparable set of random series.

4. Results

We first present the results for the 400 kyr long dataset from the Vostok ice core in Antarctica, then the 120 kyr record from the NGRIP ice core in Greenland, and third, a short, 20 kyr long global deglaciation dataset supplied by Shakun et al. (2012). Lastly, we compare the results for the three datasets.

4.1. Antarctica, period 400 ka to present

For Antarctica, temperature and CO_2 follow each other closely. The LOESS smoothed values are closely correlated: $T = -558 + 0.416 \times \text{CO}_2$, $R^2 = 0.85$, $p < 0.001$, and $n = 802$ (Fig. 3A). Temperature is mainly a leading variable to CO_2 , but there are exceptions shown as negative bars in Fig. 3C. During the period 396 ka to 358 ka, CO_2 was mainly leading temperature. This was also the case during short-term periods with small amplitude temperature changes: 214–209 ka, 268–259 ka, 202–199 ka, 172–157 ka, 101–92 ka, and 54–43 ka. The periods are marked in red in Fig. 3A. Significant short-term pauses lasted 8.7 ± 4.3 kyr (Fig. 3C). During 5 of those 6 hiatus periods, CO_2 levels off before temperatures decrease. It is only possible to define common cycles and phase shifts for CO_2 and temperature during 17% of the time. During the periods where cycles can be defined, there are periods where there are distinct cycles between CO_2 and temperature, that is, the cycles are long (> 7 –11 time steps) and therefore probably not due to stochastic movements in the two series. These cycles are 84 ± 82 kyr long, probably corresponding to the glacial-interglacial cycles. The phase shift between CO_2 and temperature is 6.1 ± 14.1 kyr.

The results for methane, CH_4 , are not as distinct as for CO_2 . However, also for methane, it appears that temperature lags CH_4 during ice-age periods and during the short-term pauses. Supplementary material 3 shows results for methane. The periods where common cycle lengths for CH_4 and temperature can be defined corresponding to the periods where there are common cycle lengths for CO_2 and temperature. We also examined the relation between CO_2 and CH_4 . For 61% of the time, CO_2 significantly lagged CH_4 (Supplementary material 4).

To investigate whether our results are robust, we also applied the LL

method to the dataset by Parrenin et al. (2013). The data were pre-treated like the Vostok ice-core data. The results largely confirm the Vostok core data results, in particular the results for the short-term pauses. The results are shown in Supplementary material 5.

4.2. Greenland, period 120 ka to present

The period with data from the Greenland ice core starts at 120 ka and thus includes a cooling and a deglaciation sequence (Fig. 3B). The Greenland ice core is too acid to allow identification of CO_2 (Delmas, 1993). We therefore assume that the CO_2 values obtained from the Antarctica core are global and compare temperatures from Greenland with global CO_2 values. CO_2 -A and TEMP-G are closely correlated: $\text{CO}_2\text{-A} = 0.925 \times \text{TEMP-G}$, $R^2 = 0.86$, $p < 0.001$, and $n = 240$. In the beginning of the cooling period, the temperature leads CO_2 . However, during the first short-term pauses, there is a short period when CO_2 leads temperature. During the cold period, CO_2 becomes a consistent leading variable to the temperature for 27 kyr (68 ka to 41 ka). Thereafter, CO_2 mainly lags temperature (Fig. 3D). The average cycle lengths are 37.2 ± 34.0 kyr, and the phase shift is 4.2 ± 7.7 kyr. Note that CO_2 and temperature are in-phase during the time window 103.5 ka to 79 ka ($\beta = 0.75$) but are anti-phase during the time window 61 ka to 41 ka ($\beta = -0.67$).

4.3. The global deglaciation period 22 ka–6 ka

The normalized and LOESS smoothed data for the second order polynomial detrended global deglaciation period are shown in Fig. 4A. We have chosen to apply a degree of smoothing that preserved the two characteristic peaks at the end of the period. The two raw series were significantly correlated ($\text{CO}_2 = 0.911 \times T$, $R^2 = 0.968$, $p < 0.001$, and $n = 153$) as were the detrended series ($\text{CO}_2 = 0.506 \times T$, $R^2 = 0.506$, $p < 0.001$, and $n = 153$). The red dots in this figure will be discussed below. The global temperature as well as CO_2 shows a two-step rise that translates into a two-peak pattern in the detrended series. The first peak is at 14 ka, that is during the Bølling-Allerød phase, and the second peak occurs at 10 ka during the Holocene, cf. graphs in Shakun et al. (2012). Carbon dioxide, CO_2 , appears to be consistently leading temperature from approximately 20.1 ka to 6 ka, with the exception of a short period from 15.1 ka to 15.4 ka. Thus, CO_2 is leading during both peaks periods (Fig. 4C). During the full period, CO_2 leads temperature significantly 92% of the time.

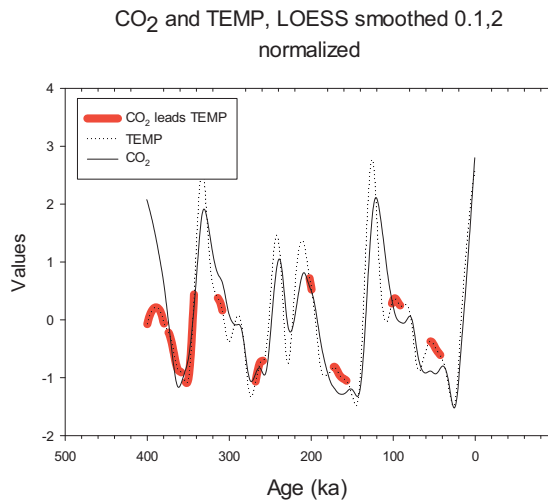
The significant cycle lengths we find with the LL method are in the range 20 to 40 time steps. One time step corresponds to 100 years, and thus cycle lengths are 2 to 4 kyr (3.3 ± 3.4 kyr). This compares well with the distance between the peaks in Fig. 4A shown by the red dots. This range of cycle length can be compared to cycle lengths for the series found in the PSD of Antarctica and Greenland series (time steps here are 500 years, Fig. 1C and D). There are several shorter cycles of 6 to 8 time steps (3 to 4 kyr) found in the PSD graphs corresponding to the common cycle lengths found with the LL method. There are also cycles of 17 and 26 time steps for CO_2 and temperature in Antarctica corresponding to 8.5 kyr and 13 kyr. The phase shift is 0.9 ± 0.6 kyr. There are cycles of 17 and 23 steps for temperature and CH_4 corresponding to 8.5 kyr and 11.5 kyr. For cycles defined by the cumulative angle method (the saw-toothed patterns in Fig. 4E), the cycle lengths are approximately 3–4 kyr.

4.4. Temperatures in Antarctica and Greenland

Antarctic temperature generally leads Greenland temperature. However, there are a few exceptions, as shown in Fig. 4B and D. In particular, Antarctic temperature leads Greenland temperature just preceding the Bølling-Allerød period from 14.7 ka to 12.7 ka. (Since our smoothing algorithm removed the B-A pattern, we included the raw series of the B-A pattern in Figs. 3B and 4B.) Note that TEMP-A and

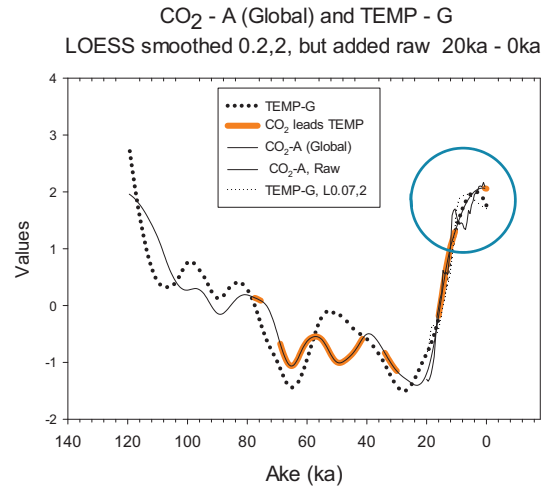
Antarctic, CO₂ -A TEMP - A

A

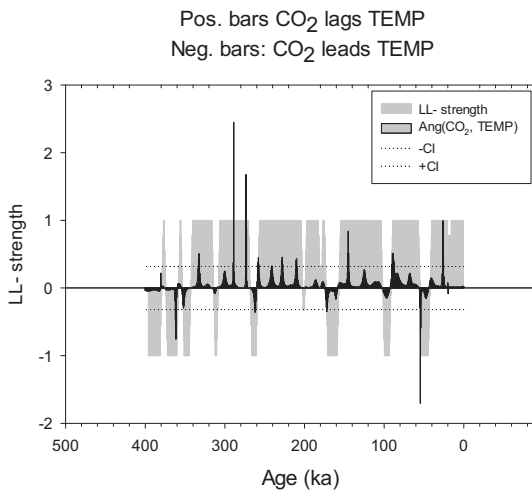


Greenland, «Global CO₂», TEMP - G

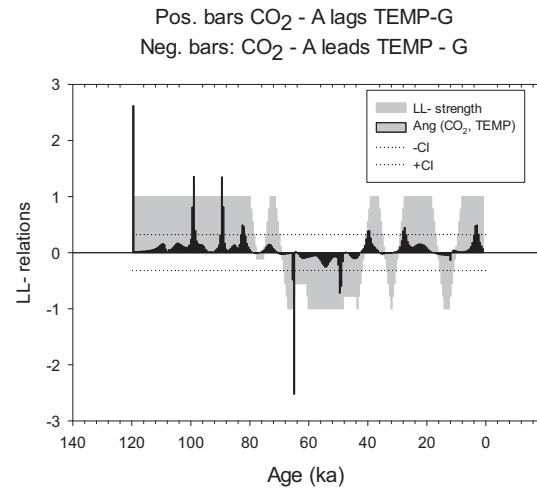
B



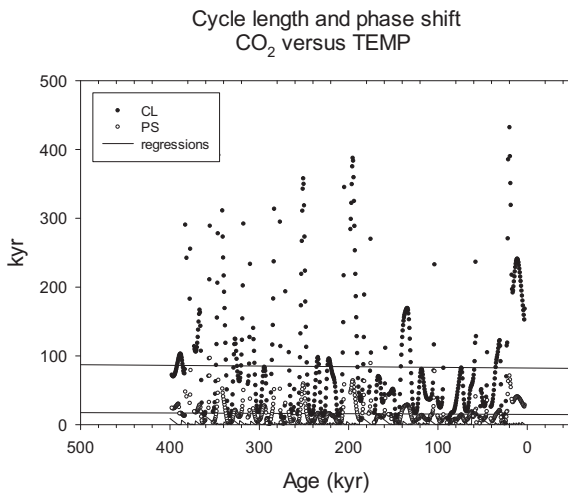
C



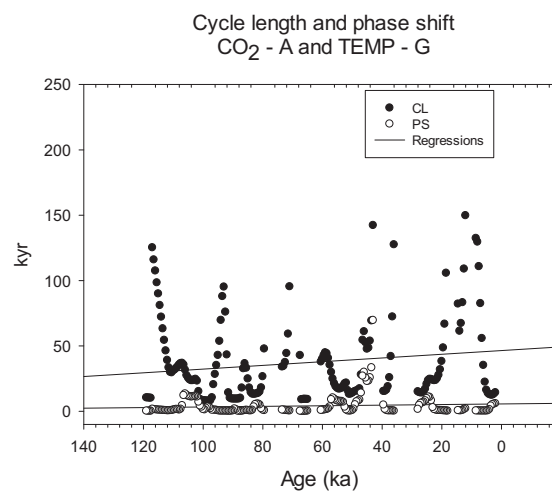
D



E



F



(caption on next page)

Fig. 3. Leading and lagging relations for smoothed CO₂ and smoothed temperature (TEMP) for time series from the Antarctic (left column) and from Greenland (right column). A. Antarctic: CO₂ and temperature series normalized to unit standard deviation. B. Greenland: CO₂ and temperature series. The circle shows a section where raw data has been included. C. Antarctic: Leading-lagging LL-relations as angles (black bars). The gray bars show LL strength relative to confidence limits (–CI, +CI). D. Greenland: The gray bars show LL relations relative to confidence limits (–CI, +CI), and the black bars show angles. E. Antarctic: Cycle length and phase shift. Cycle lengths, black dots > 500 kyr have been removed, the average cycle length is 89 ± 100 kyr (178 time steps) and the average phase shift is 17 ± 17 kyr. F. Greenland: Cycle length and phase shift. Cycle lengths, black dots > 250 kyr have been removed. The average cycle length is 37.2 ± 34.0 kyr, and the average phase shift is 7.6 ± 6.5 kyr.

TEMP-G are in phase from 103.5 ka to 79 ka but are anti-phase from 61 ka to 41 ka.

The partial ellipse method identifies cycle lengths of 31 ± 21 kyr, whereas the cumulative angle method identifies common cycles of 35 kyr to 44 kyr. The PSD graphs for Antarctic and Greenland identify a common cycle at ≈ 12–13 kyr. Thus, the short cycles found in the PSD graphs are also identified as common cycles for CO₂ and temperature. The cycle lengths correspond fairly well with the distance between peaks in the series (Fig. 4B). Phase shifts were on average 2.4 kyr (4.6 ± 6.2 time steps).

5. Discussion

We first discuss the results for the Vostok core data from Antarctica and for the NGRIP data from Greenland. Thereafter, we discuss the last global deglaciation period based on the data compiled by Shakun et al. (2012). Lastly, we compare results based on the three datasets.

For both the Antarctica series and Greenland series, CO₂ tends to be a leading variable to temperature during the coldest part of the ice ages and in short-term pauses during cooling. The Bølling-Allerød interstadial, 14.7 ka to 12.7 ka, is included in an apparent short-term pause. CO₂ appears as a lagging variable during warm periods. Generally, the Antarctic temperatures lead the Greenland temperatures.

5.1. Antarctica, period 400 ka to present

We find that different LL relations between temperature, carbon dioxide, CO₂, and methane, CH₄, govern the cool glacial periods and the subsequent warm periods during the last 400 kyr. The glacial periods contain slowly cooling sequences typically lasting 60 kyr that are sometimes interrupted by short-term pauses lasting on average 8.7 ± 4.3 kyr and thereafter followed by rapid deglaciation periods typically lasting 20 kyr.

During the cool part of the ice ages, or during periods where freezing is halted, i.e., during the short-term pauses, CO₂ comes before temperature. The pattern repeats itself during the four ice ages included in the Antarctica 400 kyr series (Fig. 3A and C). Both the Vostok core series and the Parrenin et al. (2013) series (Supplementary material 5) show the characteristic patterns for CO₂ and temperature, but in the Parrenin series, there are also short-time windows during glaciation (≈ 200 ka) and deglaciation (≈ 130 ka) when CO₂ appears to lead temperature. We believe that the results for the hiatus-like time windows are more robust than the results for the rapid glaciation and deglaciation periods because the phase shift is more easily detected during slow temperature and CO₂ changes.

The short-term pauses can be compared to the return time for the last glacial Antarctic warming events (Antarctic isotope maximum, AIM) of 6 to 10 kyr identified by Kawamura et al. (2017). These events also occurred during the seven interglacial stages from 700 ka to present.

The cycle lengths for the four ice ages were approximately 90 kyr, corresponding to the cycle lengths that can be identified visually in Fig. 3A and to the cycle lengths of 100 kyr identified in several studies (e.g., Imbrie et al. (1992); Loulergue et al. (2008) for CH₄). Phase shifts between CO₂ and temperature were approximately 6.2 ± 14.1 kyr over the whole period. The shifts are smaller than the time constant of approximately 15 kyr required for climate inertia to produce 100 kyr

cycles suggested by Imbrie et al. (1993). Furthermore, the shift can be compared to the smaller uncertainties in the gas-age differences of 0.4 to 0.6 kyr (Parrenin et al., 2013), supporting the LL relations as real.

Our results for the four ice ages contrast with earlier results. For example, Stips et al. (2016) found that on palaeoclimate time scales of ≈ 800 ka, temperature changes cause subsequent CO₂/CH₄ changes. Over more recent time windows, both Cuffey and Vimeux (2001) and Parrenin et al. (2013) found that CO₂ and temperature change synchronously. It is interesting that methane leads CO₂ 61% of the time because the causes for CH₄ variation are quite probably different from the causes for CO₂ variations. For example, Monnin et al. (2001) and Alley et al. (2002) suggest that CH₄ is probably related to wetland expansion. Loulergue et al. (2008) add volatile organic compound emissions from tropical forests. However, CO₂ is related to deep-water ocean circulations. In addition to giving a description of the CO₂-temperature relations during the last 400 kyr, the results also support the dating of the time series.

One method to validate the chronology in ice-core time series is to tie events in the series to endogenous events (e.g., geomagnetic events and volcanic dust records (Kawamura et al., 2017)). Here, we identify a pattern of events related to the interaction between CO₂ and temperature, which repeats itself during four successive glaciation periods. If the time series for temperature and CO₂ (data are observed at two different time scales) had been in error, the LL relations for CO₂/temperature would probably not repeat for each ice age.

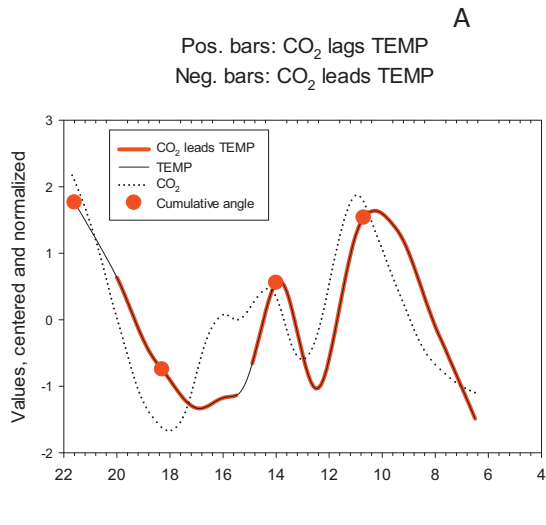
5.2. Greenland, period 120 ka to present

For the Greenland series, we do not have CO₂ observations because the ice cores are acidic and have large impurity contents (Barnola et al., 1995). We therefore used the CO₂ values found in the Antarctica core as representative for CO₂ in the global atmosphere. The LL relations between CO₂ and temperature seem to show similar patterns in Antarctica as in Greenland, supporting the finding that the CO₂ values found in the Vostok ice core are representative for CO₂ in the global atmosphere. The Greenland time series tell the same story as Antarctica time series for the last cooling period and the subsequent warming period. During the cool period and short-term pauses, CO₂ and CH₄ lead the temperature. Our estimates based on the common cycle lengths for CO₂ and TEMP show that the cycle length of 37.7 ± 34 kyr is a little less than the orbital frequencies of 41 kyr reported by Loulergue et al. (2008): 100, 41, 23 and 19 kyr for methane.

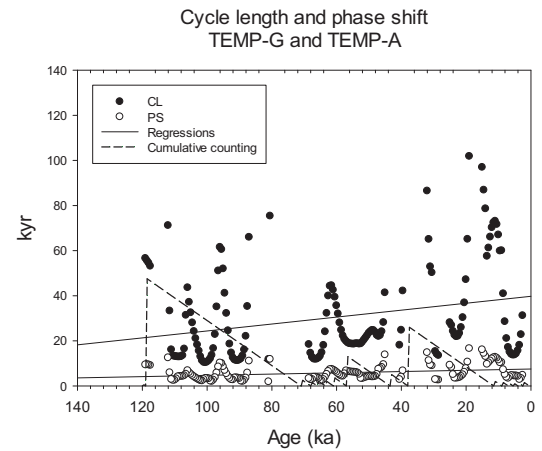
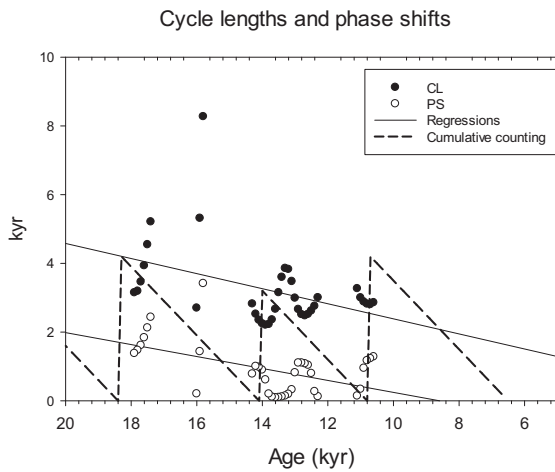
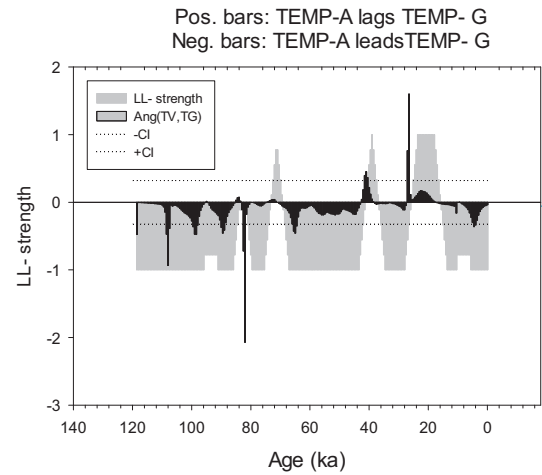
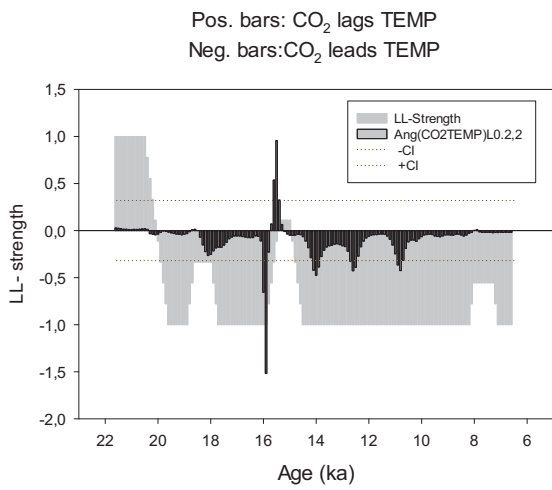
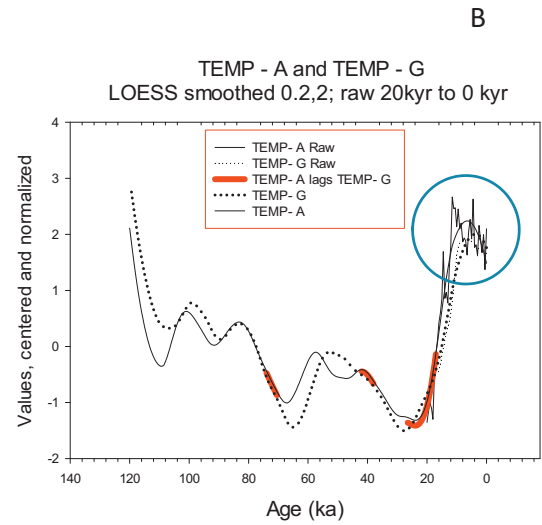
There are three time windows that show different and contrasting patterns in the Greenland series: the first period is from 103.5 ka to 79 ka, the second period is from 61.5 ka to 43.5 ka, and the third period is from 18 ka to 8.5 ka. During the *first* of these periods, 103.5 ka to 79 ka, both CO₂ and TEMP-A are in phase with TEMP-G ($\beta = 1.1$ and $\beta = 0.75$). During the *second* period, 61.5 ka to 43.5 ka, CO₂ and TEMP-G are in antiphase ($\beta = -0.86$), and TEMP-A and TEMP-G are in antiphase ($\beta = -0.65$). The data do not allow for a physical explanation of this difference, but the second period is closer to the turning point for deglaciation.

The *third* time window starts during the last deglaciation period at approximately 18 ka and ends at approximately 8.5 ka. During this period, which includes the Bølling-Allerød, B-A, warming period from 14.7 ka to 12.7 ka, CO₂ leads temperature. At the start of this period, at 14 ka, Lora et al. (2016) found that there was a rapid loss of ice that

Global glaciation, CO₂ and TEMP



TEMP Antarctica vs. TEMP Greenland



(caption on next page)

Fig. 4. Leading and lagging relations. A. Time series from global composite smoothed CO₂ and smoothed temperature (TEMP) normalized to unit standard deviation. The red dots show the start and end of the cumulative counting of angles until the sum is 2π . B. Northern and Southern Hemispheres: temperature series. The circle indicates the section where raw series were included to see details. C. Global composite: Leading–lagging LL relations as angles. The gray bars show LL strength relative to confidence limits ($-CI$, $+CI$), and the black bars show angles. D. Northern and Southern Hemispheres: The gray bars show LL strength relative to confidence limits ($-CI$, $+CI$), and the black bars show angles. E. Global composite: Cycle length and phase shift. Cycle lengths, black dots > 10 kyr have been removed. The cycle lengths are $3.3 \text{ kyr} \pm 3.4$ (time steps 33 ± 34), and the phase shifts are 0.8 ± 0.6 kyr. F. Northern and Southern Hemispheres: Cycle length and phase shift. Cycle lengths, black dots > 200 kyr have been removed. The cycle lengths are 30.5 ± 20.5 kyr (61 and 41 time steps), and the phase shifts are 5.8 ± 3.3 kyr. (For interpretation of the references to color in this figure legend, the reader is referred to the web version of this article.)

caused an abrupt reorganization of North Pacific and Western North American ocean circulations. Su et al. (2016) have shown that upwelling of warm salty water to the surface in the North Atlantic may have contributed to the warming. During a period that just precedes the period where CO₂ leads temperature, 25.5 ka to 17 ka, there is also a shift such that the Southern Hemisphere temperature lags the Northern Hemisphere temperature, i.e., TEMP–A lags TEMP–G.

5.3. The global deglaciation period, 22 ka–6 ka

Our results for the deglaciation period are based on the time series for global deglaciation supplied by Shakun et al. (2012) and correspond well with the results found by Shakun et al. (2012). We use data for CO₂ transferred to AICC2012. They show that increasing CO₂ concentrations are either synchronous or preceding global warming during the last deglaciation, that is, 22 ka to approximately 6 ka. They found that the period when CO₂ consistently leads temperature starts at 17.5 ka, and they conclude that CO₂ was therefore not the cause of initial warming. We found that CO₂ mostly leads temperature by 22 ka but that there is a short period of 15.4 ka to 15.1 ka, during which TEMP leads CO₂ by 0.9 ± 0.6 kyr.

These results support our *first* hypothesis that CO₂ and temperature shift between being leading and lagging variables in Antarctica and in Greenland. Both in Antarctica and Greenland, a leading role for CO₂ appears to be almost but not exclusively related to a decrease in CO₂ and a short-term pause in temperature change. The temperatures in Antarctica are leading the temperatures in the Northern Hemisphere. The mechanisms causing this pattern have been discussed (e.g., He et al. (2013); Alley et al. (2002)). However, there are short periods during which the LL relation is reversed, in particular from 26 ka to 17 ka, that is, at the turning point for the last deglaciation period.

Our *second* hypothesis was only partially supported. The patterns we found for the short-term pauses in the Antarctica series were also found in the Greenland series. However, there also seem to be short-term pauses associated with deglaciation (the B–A period and its extension). As with the other short-term pauses, there is a change in the LL roles of CO₂ and temperature. The reason that short term pauses were not shown during the Antarctic deglaciation may be that the resolution is too small (500 years). Neither did we see pronounced changes in LL roles for CO₂ and temperature in the global dataset. However, such changes may still be present because the series do not include much of the preceding glaciation.

There is one caveat to the interpretation of the LL relations. Since both heat transfer in the ocean and warming caused by CO₂ in the atmosphere impact surface temperatures, temperature changes related to ocean heat transfer may cause the global (and hemisphere) temperature anomalies to peak before CO₂ peaks. Further disentangling the effects of ocean heat warming and warming caused by CO₂ should therefore be an important issue.

5.4. Antarctica and Greenland compared

There are close connections between temperature variations in Antarctica and the Arctic, and the term ‘see-saw’ has been used to describe an apparent inverse relation between peaks and troughs in temperature variations between the two hemispheres (Broecker, 1998;

Stocker, 1998; Chylek et al., 2010). The term ‘see-saw’ is used for two distinct antiphase events. Here, we add a third phenomenon that shows a see-saw-like pattern and that also shows a particular LL relation with CO₂.

5.4.1. The bipolar see-saw

First, a twentieth century antiphase pattern in the multidecadal temperature anomalies in the Arctic and Antarctic regions was identified by Chylek et al. (2010) as a bipolar see-saw. The cycle length was estimated to be 70 years. Second, a multimillennial antiphase pattern was identified and given a physical rationale by Stocker and Johnsen (2003) and Siddall et al. (2006). The antiphase pattern lasted from between 60 ka and 25 ka and showed cycle lengths of approximately 1.5–2 kyr. Third, in the present study, we find a see-saw-like pattern in the smoothed time series between approximately 60 ka and 40 ka. The cycle length is approximately 20 kyr. Furthermore, there is a see-saw pattern, i.e., an anti-phase between CO₂ and Greenland temperature; that is, when the Greenland temperature shows a peak, CO₂ shows a trough, similar to in the Antarctic region.

There are several explanations for the see-saw phenomenon. The Atlantic meridional overturning has a role in most explanations (e.g., Wang et al. (2015)), but Yao et al. (2017) assign a role for multiple ocean surface temperatures. The effect of ocean warming in addition to the role of greenhouse gases (GHG) may explain some of the changes between leading and lagging roles for CO₂ and temperature. For example, the increase in Northern Hemisphere warming during the period 1980 to 2009 (Wang et al., 2015; Yao et al., 2017) may contribute to a global temperature anomaly (GTA), being a leading variable to CO₂ during the period 1980 to 2010 (Kuo et al., 1990; Seip and Grøn, 2017a, 2017b).

For the two time windows 103.5 to 79 ka and 60 to 41 ka that both include approximately one cycle in temperature and CO₂, there are differences in their leading – lagging patterns. We suggest that in the see-saw context for Northern and Southern Hemisphere temperatures, the most likely explanation is that TEMP–A leads TEMP–G (as seen visually and numerically in Fig. 4B, the time window 103 ka to 79 ka) but that the lag time for TEMP–G is larger during the time window from 61 ka to 41 ka, producing a see-saw-like pattern. LL relations just express the time it takes a process to impact a second process relative to their (common) cycle lengths, but normally the term “leading” is restricted to series that peak less than $\frac{1}{4} \lambda$ before the response series peak. The term ‘see-saw’ suggests that the process can go both ways. It would be interesting to examine if the see-saw signature in general also implies an antiphase between CO₂ and Greenland temperature.

Based on the descriptions of causes for the glaciation-deglaciation processes as interactions between large global regions (land and oceans), it would be tempting to invoke both a control knob (e.g., orbital frequencies) and a cellular automata mechanism (Fleming, 2017). With the latter mechanism, fractal like patterns may occur and indicate short-term pauses and see-saw effects.

5.5. The method

There is no canonical rule for identifying time series that represent candidate causes and effects within series that consist of superimposed signals. For example, some interactions may result in time series that

express dynamic chaos and thus be impossible to extract uniquely (e.g., Sugihara and May (1990); Tømte et al. (1998)). To our knowledge, most previous decomposition methods examine one series at a time. With the present method, we identify LL relations between paired series. If the two series show consistent LL relations for > 7 time steps, the assumption that the two series represent real processes that are causally related is strengthened. LL relations for longer than 7 time steps have a probability of being caused by chance of $p < 0.05$ (Seip and Grøn, 2017a, 2017b).

A possibility remains that our findings are artifacts of the dating uncertainties and of the method. However, the LL pattern we found for CO₂ and temperature is robust with respect to single core (the Vostok ice core) and multiple core time series (Parrenin et al., 2013). The method is conceptually simple, and the numerical values for LL relations can often be seen to correspond with the LL relations shown in the time series. Furthermore, in the Antarctica time series, we see similar patterns repeat with each glaciation period. This indicates that the method provides correct results.

6. Conclusions

The leading-lagging method presented here allows for detailed examinations of LL relations between paired time series for global warming variables. Applying the method to palaeontological time series from Antarctica and Greenland shows that there are several periods where carbon dioxide, CO₂, leads temperature even if the main pattern is that temperature is a leading variable to CO₂. The CO₂ leading periods can be associated with events in the Southern and Northern Hemisphere temperature anomalies. In particular, we find that CO₂ leads temperature during short-term pauses in the glaciation-deglaciation sequence. During the recent deglaciation period, CO₂ leads temperature during the Bølling-Allerød warming, which, together with the following Younger Dryas period, appears as a short-term pause in temperature change during the last deglaciation. We find that there is also a see-saw pattern on a multi-millennial time scale and that this see-saw pattern is accompanied by an antiphase pattern for CO₂ relative to the Greenland temperature.

Data availability

The data and all calculations can be obtained from the first author.

Appendix A. Supplementary data

Supplementary data to this article can be found online at <https://doi.org/10.1016/j.palaeo.2018.06.021>.

References

- Alley, R.B., Brook, E.J., Anandakrishnan, S., 2002. A northern lead in the orbital band: north-south phasing of Ice-Age events. *Quat. Sci. Rev.* 21 (1–3), 431–441.
- Barker, S., Knorr, G., Edwards, R.L., Parrenin, F., Putnam, A.E., Skinner, L.C., Wolff, E., Ziegler, M., 2011. 800,000 years of abrupt climate variability. *Science* 334 (6054), 347–351.
- Barnola, J.M., Ankin, M., Porcheron, J., Raynaud, D., Schwander, J., Stauffer, B., 1995. CO₂ evolution during the last millennium as recorded by Antarctic and Greenland ice. *Tellus Ser. B Chem. Phys. Meteorol.* 47 (1–2), 264–272.
- Broecker, W.S., 1998. Paleocirculation during the last deglaciation: a bipolar seesaw? *Paleoceanography* 13 (2), 119–121.
- Buizert, C., Adrian, B., Ahn, J., Albert, M., Alley, R.B., Baggenstos, D., Bauska, T.K., Bay, R.C., Bencivengo, B.B., Bentley, C.R., Brook, E.J., Chellman, N.J., Clow, G.D., Cole-Dai, J., Conway, H., Cravens, E., Cuffey, K.M., Dunbar, N.W., Edwards, J.S., Fegyveresi, J.M., Ferris, D.G., Fitzpatrick, J.J., Fudge, T.J., Gibson, C.J., Gkinis, V., Goetz, J.J., Gregory, S., Hargreaves, G.M., Iverson, N., Johnson, J.A., Jones, T.R., Kalk, M.L., Kippenhan, M.J., Koffman, B.G., Kreutz, K., Kuhl, T.W., Lebar, D.A., Lee, J.E., Marcott, S.A., Markle, B.R., Maselli, O.J., McConnell, J.R., McGwire, K.C., Mitchell, L.E., Mortensen, N.B., Neff, P.D., Nishiizumi, K., Nunn, R.M., Orsi, A.J., Pasteris, D.R., Pedro, J.B., Pettit, E.C., Price, P.B., Priscu, J.C., Rhodes, R.H., Rosen, J.L., Schauer, A.J., Schoenemann, S.W., Sendelbach, P.J., Severinghaus, J.P., Shturmakov, A.J., Sigl, M., Slawny, K.R., Souney, J.M., Sowers, T.A., Spencer, M.K., Steig, E.J., Taylor, K.C., Twickler, M.S., Vaughn, B.H., Voigt, D.E., Waddington, E.D., Welten, K.C., Wendricks, A.W., White, J.W.C., Winstrup, M., Wong, G.J., Woodruff, T.E., Members, W.D.P., 2015. Precise interglacial phasing of abrupt climate change during the last ice age. *Nature* 520 (7549), 661–U169.
- Chylek, P., Folland, C.K., Lesins, G., Dubey, M.K., 2010. Twentieth century bipolar seesaw of the Arctic and Antarctic surface air temperatures. *Geophys. Res. Lett.* 37.
- Cuffey, K.M., Vimeux, F., 2001. Covariation of carbon dioxide and temperature from the Vostok ice core after deuterium-excess correction. *Nature* 412 (6846), 523–527.
- Delmas, R.J., 1993. A natural artifact in Greenland ice-core CO₂ measurements. *Tellus Ser. B Chem. Phys. Meteorol.* 45 (4), 391–396.
- DeVries, T., Holzer, M., Primeau, F., 2017. Recent increase in carbon uptake driven by weaker upper-ocean overturning. *Nature* 542, 215–220.
- Ellner, S.P., Turchin, P., 2005. When can noise induce chaos and why does it matter: a critique. *Oikos* 111 (3), 620–631.
- Fleming, S.W., 2017. *Where the River Flows: Scientific Reflections on Earth's Waterways*. Princeton University Press, Princeton, New Jersey.
- Granger, C.W.J., 1969. Investigating causal relations by econometric models and cross-spectral methods. *Econometrica* 37 (3), 424–438.
- He, F., Shakun, J.D., Clark, P.U., Carlson, A.E., Liu, Z.Y., Otto-Bliesner, B.L., Kutzbach, J.E., 2013. Northern Hemisphere forcing of Southern Hemisphere climate during the last deglaciation. *Nature* 494 (7435), 81–85.
- Huang, N.E., Shen, Z., Long, S.R., Wu, M.L.C., Shih, H.H., Zheng, Q.N., Yen, N.C., Tung, C.C., Liu, H.H., 1998. The empirical mode decomposition and the Hilbert spectrum for nonlinear and non-stationary time series analysis. *Proc. R. Soc. A Math. Phys. Eng. Sci.* 454 (1971), 903–995.
- Huybers, P., Langmuir, C., 2009. Feedback between deglaciation, volcanism, and atmospheric CO₂. *Earth Planet. Sci. Lett.* 286 (3–4), 479–491.
- Huybers, P., Langmuir, C.H., 2017. Delayed CO₂ emissions from mid-ocean ridge volcanism as a possible cause of late-Pleistocene glacial cycles. *Earth Planet. Sci. Lett.* 457, 238–249.
- Imbrie, J., Boyle, E.A., Clemens, S.C., Duffy, A., Howard, W.R., Kukla, G., Kutzbach, J., Martinson, D.G., McIntyre, A., Mix, A.C., Molino, B., Morley, J.J., Peterson, L.C., Pisias, N.G., Prell, W.L., Raymo, M.E., Shackleton, N.J., Toggweiler, J.R., 1992. On the structure and origin of major glaciation cycles 1. Linear responses to Milankovitch forcing. *Paleoceanography* 7 (6), 701–738.
- Imbrie, J., Berger, A., Boyle, E.A., Clemens, S.C., Duffy, A., Howard, W.R., Kukla, G., Kutzbach, J., Martinson, D.G., McIntyre, A., Mix, A.C., Molino, B., Morley, J.J., Peterson, L.C., Pisias, N.G., Prell, W.L., Raymo, M.E., Shackleton, N.J., Toggweiler, J.R., 1993. On the structure and origin of major glaciation cycles. 2. The 100,000-year cycle. *Paleoceanography* 8 (6), 699–735.
- Johnston, T.C., Alley, R.B., 2006. Possible role for dust or other northern forcing of ice-age carbon dioxide changes. *Quat. Sci. Rev.* 25 (23–24), 3198–3206.
- Kawamura, K., Abe-Ouchi, A., Motoyama, H., Ageta, Y., Aoki, S., Azuma, N., Fujii, Y., Fujita, K., Fujita, S., Fukui, K., Furukawa, T., Furusaki, A., Goto-Azuma, K., Greve, R., Hirabayashi, M., Hondoh, T., Hori, A., Horikawa, S., Horiuchi, K., Igarashi, M., Izuka, Y., Kameda, T., Kanda, H., Kohno, M., Kuramoto, T., Matsushi, Y., Miyahara, M., Miyake, T., Miyamoto, A., Nagashima, Y., Nakayama, Y., Nakazawa, T., Nakazawa, F., Nishio, F., Obinata, I., Ohgaito, R., Oka, A., Okuno, J., Okuyama, J., Oyabu, I., Parrenin, F., Pattyn, F., Saito, F., Saito, T., Saito, T., Sakurai, T., Sasa, K., Seddik, H., Shibata, Y., Shinbori, K., Suzuki, K., Suzuki, T., Takahashi, A., Takahashi, K., Takahashi, S., Takata, M., Tanaka, Y., Uemura, R., Watanabe, G., Watanabe, O., Yamasaki, T., Yokoyama, K., Yoshimori, M., Yoshimoto, T., Project, D.F.I.C., 2017. State dependence of climatic instability over the past 720,000 years from Antarctic ice cores and climate modeling. *Sci. Adv.* 3 (2).
- Kestin, T.S., Karoly, D.J., Yang, J.L., Rayner, N.A., 1998. Time-frequency variability of ENSO and stochastic simulations. *J. Clim.* 11 (9), 2258–2272.
- Knutson, T.R., Sirutis, J.J., Zhao, M., Tuleya, R.E., Bender, M., Vecchi, G.A., Villarini, G., Chavas, D., 2015. Global projections of intense tropical cyclone activity for the late twenty-first century from dynamical downscaling of CMIP5/RCP4.5 scenarios. *J. Clim.* 28 (18), 7203–7224.
- Kuo, C., Lindberg, C., Thomson, D.J., 1990. Coherence established between atmospheric carbon-dioxide and global temperature. *Nature* 343 (6260), 709–714.
- Lora, J.M., Mitchell, J.L., Tripathi, A.E., 2016. Abrupt reorganization of North Pacific and western North American climate during the last deglaciation. *Geophys. Res. Lett.* 43 (22), 11796–11804.
- Loulergue, L., Schilt, A., Spahni, R., Masson-Delmotte, V., Blunier, T., Lemieux, B., Barnola, J.M., Raynaud, D., Stocker, T.F., Chappellaz, J., 2008. Orbital and millennial-scale features of atmospheric CH₄ over the past 800,000 years. *Nature* 453 (7193), 383–386.
- Luthi, D., Le Floch, M., Bereiter, B., Blunier, T., Barnola, J.M., Siegenthaler, U., Raynaud, D., Jouzel, J., Fischer, H., Kawamura, K., Stocker, T.F., 2008. High-resolution carbon dioxide concentration record 650,000–800,000 years before present. *Nature* 453 (7193), 379–382.
- Ma, C., Meyers, S.R., Sageman, B.B., 2017. Theory of chaotic orbital variations confirmed by Cretaceous geological evidence. *Nature* 542, 408–470.
- Monnin, E., Indermuhle, A., Dallenbach, A., Fluckiger, J., Stauffer, B., Stocker, T.F., Raynaud, D., Barnola, J.M., 2001. Atmospheric CO₂ concentrations over the last glacial termination. *Science* 291 (5501), 112–114.
- Parrenin, F., Masson-Delmotte, V., Kohler, P., Raynaud, D., Paillard, D., Schwander, J., Barbante, C., Landais, A., Wegner, A., Jouzel, J., 2013. Synchronous change of atmospheric CO₂ and Antarctic temperature during the last deglacial warming. *Science* 339 (6123), 1060–1063.
- Patra, P.K., Maksyutov, S., Ishizawa, M., Nakazawa, T., Takahashi, T., Ukita, J., 2005. Interannual and decadal changes in the sea-air CO₂ flux from atmospheric CO₂ inverse modeling. *Glob. Biogeochem. Cycles* 19 (4).
- Petit, J.R., Jouzel, J., Raynaud, D., Barkov, N.L., Barnola, J.M., Basile, I., Bender, M., Chappellaz, J., Davis, M., Delaygue, G., Delmotte, M., Kotlyakov, V.M., Legrand, M.,

- Lipenkov, V.Y., Lorius, C., Pepin, L., Ritz, C., Saltzman, E., Stievenard, M., 1999. Climate and atmospheric history of the past 420,000 years from the Vostok ice core, Antarctica. *Nature* 399 (6735), 429–436.
- Seip, K.L., Grøn, O., 2016. Leading the game, losing the competition: identifying leaders and followers in a repeated game. *PLoS One* 11 (3).
- Seip, K.L., Grøn, Ø., 2017a. A new method for identifying possible causal relationships between CO₂, total solar irradiance and global temperature change. *Theor. Appl. Climatol.* 127, 923–938.
- Seip, K.L., Grøn, Ø., 2017b. On the statistical nature of distinct cycles in global warming variables. *Clim. Dyn.*
- Seip, K.L., McNowin, R., 2007. The timing and accuracy of leading and lagging business cycle indicators: a new approach. *Int. J. Forecast.* 22, 277–287.
- Shakun, J.D., Clark, P.U., He, F., Marcott, S.A., Mix, A.C., Liu, Z.Y., Otto-Bliesner, B., Schmittner, A., Bard, E., 2012. Global warming preceded by increasing carbon dioxide concentrations during the last deglaciation. *Nature* 484 (7392), 49–54.
- Siddall, M., Stocker, T.F., Blunier, T., Spahni, R., McManus, J.F., Bard, E., 2006. Using a maximum simplicity paleoclimate model to simulate millennial variability during the last four glacial periods. *Quat. Sci. Rev.* 25 (23–24), 3185–3197.
- Stevens, N.T., Parizek, B.R., Alley, R.B., 2016. Enhancement of volcanism and geothermal heat flux by ice-age cycling: a stress modeling study of Greenland. *J. Geophys. Res. Earth Surf.* 121 (8), 1456–1471.
- Stips, A., Macias, D., Coughlan, C., Garcia-Gorrioz, E., San Liang, X., 2016. On the causal structure between CO₂ and global temperature. *Sci. Rep.* 6.
- Stocker, T.F., 1998. Climate change - the seesaw effect. *Science* 282 (5386), 61–62.
- Stocker, T.F., Johnsen, S.J., 2003. A minimum thermodynamic model for the bipolar seesaw. *Paleoceanography* 18 (4).
- Su, Z., Ingersoll, A.P., He, F., 2016. On the abruptness of Bolling-Allerod warming. *J. Clim.* 29 (13), 4965–4975.
- Sugihara, G., May, R.M., 1990. Nonlinear forecasting as a way of distinguishing chaos from measurement errors in time series. *Nature* 344, 731–741.
- Sugihara, G., May, R., Ye, H., Hsieh, C.H., Deyle, E., Fogarty, M., Munch, S., 2012. Detecting causality in complex ecosystems. *Science* 338 (6106), 496–500.
- Tang, Z., Shi, X.F., Zhang, X., Chen, Z.H., Chen, M.T., Wang, X.Q., Wang, H.Z., Liu, H.L., Lohmann, G., Li, P.Y., Ge, S.L., Huang, Y.H., 2016. Deglacial biogenic opal peaks revealing enhanced Southern Ocean upwelling during the last 513 ka. *Quat. Int.* 425, 445–452.
- Tømte, O., Seip, K.L., Christophersen, N., 1998. Evidence that loss in predictability (and possibly dynamic chaos) increase with increasing trophic level in aquatic ecosystems. *Oikos* 82, 325–332.
- Wang, Z.M., Zhang, X.D., Guan, Z.Y., Sun, B., Yang, X., Liu, C.Y., 2015. An atmospheric origin of the multi-decadal bipolar seesaw. *Sci. Rep.* 5.
- Wu, Z.H., Huang, N.E., Wallace, J.M., Smoliak, B.V., Chen, X.Y., 2011. On the time-varying trend in global-mean surface temperature. *Clim. Dyn.* 37 (3–4), 759–773.
- Yao, S.L., Luo, J.J., Huang, G., Wang, P.F., 2017. Distinct global warming rates tied to multiple ocean surface temperature changes. *Nat. Clim. Chang.* 7 (7), 486.